

Ensemble Simulations of Explosive Cyclogenesis at Ranges of 2–5 Days

FREDERICK SANDERS

Marblehead, Massachusetts

STEVEN L. MULLEN

Institute of Atmospheric Physics, The University of Arizona, Tucson, Arizona

DAVID P. BAUMHEFNER

National Center for Atmospheric Research, Boulder, Colorado

(Manuscript received 29 March 1999, in final form 1 February 2000)

ABSTRACT

Ensemble simulations of explosive cyclogenesis are examined in a lengthy run of a global general circulation model with the perfect ensemble context. Attention is focused on the day when the deepest low appeared. An ensemble of 31 members is obtained by integrating 30 additional runs starting from slightly perturbed initial conditions. The perturbations are randomly selected to represent equal approximations to the truth, given typical analysis differences between major centers. Ensembles are generated starting two, three, four, and five days prior to maximum depth. Two lows are contrasted, the deepest low near Kamchatka and a marginally explosive low over the central Pacific.

The early development of both systems was suppressed by their presence in the confluent entrance region of the Pacific winter jet. An intense low near Kamchatka eventually developed in each member of the ensemble at all projections, but the details of development varied from member to member and were related to the involvement of a surface perturbation coming up into the system from low latitudes. In contrast, cyclogenesis over the central Pacific occurred in some members of the ensemble but not at all in others. The difference in behavior of the two systems is reflected in a localized enhancement of the error growth of the planetary and synoptic scales for the central Pacific low and is related to the smaller horizontal scale of the central Pacific low.

Probabilistic estimates of precipitation quantity and surface wind speeds produced by the ensemble showed moderate skill at day 5 with respect to climatology, mainly away from the regions of most vigorous synoptic activity, when verified against individual ensemble members. Skill would be reduced if the ensemble mean proved to be more seriously in error as is the case for a forecast verified against observations.

1. Introduction

The sudden development of intense cyclones over the oceans of mid- and high latitudes during the cold season (Sanders and Gyakum 1980) is an important forecasting challenge, because these systems typically produce winds of gale or storm force in 24 hours or less. It has been suggested that the predictability of these storms at ranges of 1–2 days may be less than that of other less intense cyclones (Kallen and Huang 1988; Mullen and Baumhefner 1988, 1989; Kuo and Low-Nam 1990). Hence, it is desirable to evaluate the degree to which rapidly intensifying storms are sensitive to uncertainty of initial conditions at longer ranges and determine

whether the predictability of particular baroclinic structures can be different.

We have undertaken to do this by utilizing a long integration of the Community Climate Model Version 2 (CCM2) produced at the National Center for Atmospheric Research (NCAR). This model has been described by Hack et al. (1993) and was run at a spectral resolution of triangular 63 (T63). This resolution is virtually the same as that for the operational medium-range ensemble prediction system at the National Centers for Environmental Prediction (Tracton and Kalnay 1993). We studied a 180-day simulation initialized with the analysis of observations at 0000 UTC 1 October 1975. Although the resemblance of the simulation to the real atmosphere as represented by observations is surely limited to a few days (e.g., Lorenz 1982), the model appears to produce realistic-looking patterns indefinitely. Furthermore, Sanders and Mullen (1996) showed that the

Corresponding author address: Dr. Frederick Sanders, 9 Flint Street, Marblehead, MA 01945.
E-mail: FNMISander@aol.com

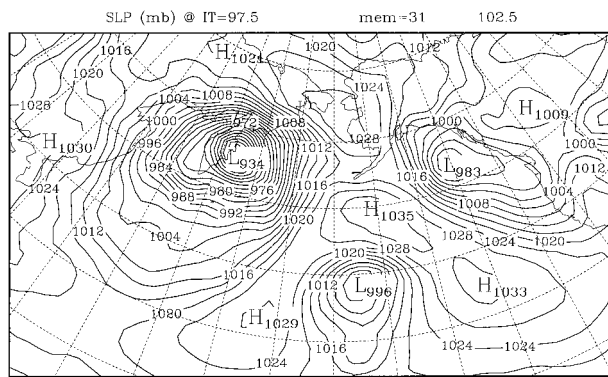


FIG. 1. Sea level isobars at intervals of 4 mb on day 102.5 for the unperturbed run starting at day 97.5. Longitude lines are at intervals of 10°, from 90°W to 110°E. Latitude lines are at intervals of 10°, from 20° to 70°N.

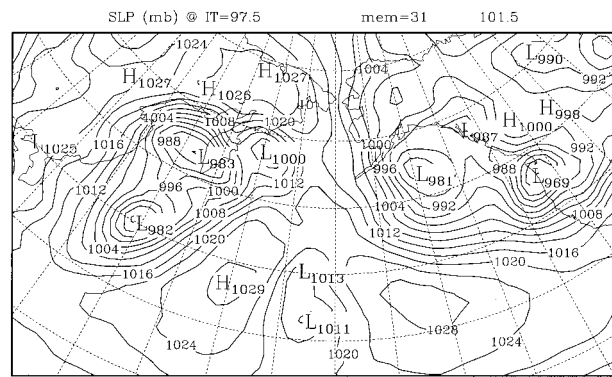


FIG. 3. Same as Fig. 1, but for day 101.5.

climatology of explosive cyclogenesis in this model was similar to that in the real atmosphere with respect to frequency, intensity, and location, suggesting that the T63 CCM2 can be used with confidence for predictability experiments.

2. Selection of case

We chose to study simulations of two to five days' duration, all verifying at day 102.5 (corresponding to a calendar date of 1200 UTC 10 January 1976) of the 180-day run. This time was the end of the largest 24-h deepening in the run, in a cyclone with a central pressure of 934 mb that lay along the east coast of the Kamchatka peninsula (Fig. 1). It was accompanied by a deep low at 500 mb (Fig. 2) almost directly overhead, flanked on its east and south sides by a strong jet.

Twenty-four hours earlier, the 985-mb cyclone was near 40°N latitude and 140°E longitude (Fig. 3). A slightly deeper low lay over the Sea of Okhotsk, just west of Kamchatka, but it lost its identity as the strongly deepening center moved up from the south-southwest.

At 500 mb (Fig. 4) a pronounced trough lay just west of the surface center, so the explosive deepening occurred in a scenario similar to that described by Sanders (1986).

A second cyclone, in the central Pacific at lower latitudes (Figs. 1 and 2) deepened just enough to qualify as a “bomb” according to the criterion of Sanders and Gyakum (1980). It was also accompanied by a pronounced 500-mb trough just upstream from the surface center. Additional deep cyclones lay in the Gulf of Alaska and over the central United States at the edge the map on day 102.5 (Fig. 1). The first of these deepened explosively over the western Pacific between days 97.5 and 98.5, while the other qualified as a bomb off the coast of Oregon in the 24-h period ending on day 101.5 (Fig. 3). These cyclones were not studied.

3. The ensembles

Four ensembles, each with 30 members, were produced by running the identical model from slightly perturbed initial conditions. The four ensembles were initiated on days 97.5, 98.5, 99.5, and 100.5, representing ranges from two to five days before the verifying day 102.5. The perturbations were obtained by the simulation of analysis differences, as described by Errico and Baumhefner (1987), Mullen and Baumhefner (1989),

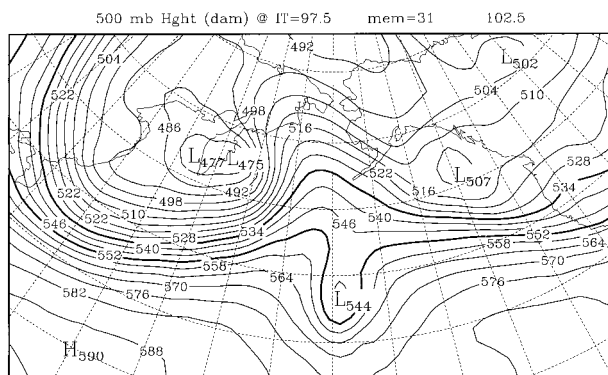


FIG. 2. 500-mb height contours at intervals of 6 dam for day 102.5 for the unperturbed run starting at day 97.5. The 534 and 552 dam contours are thickened. Latitude and longitude as in Fig. 1.

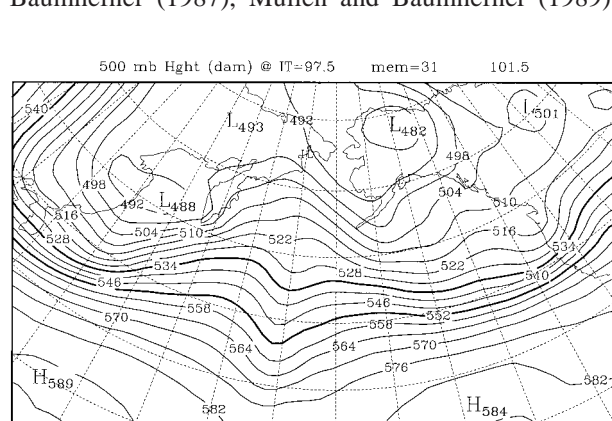


FIG. 4. Same as Fig. 2, but for day 101.5.

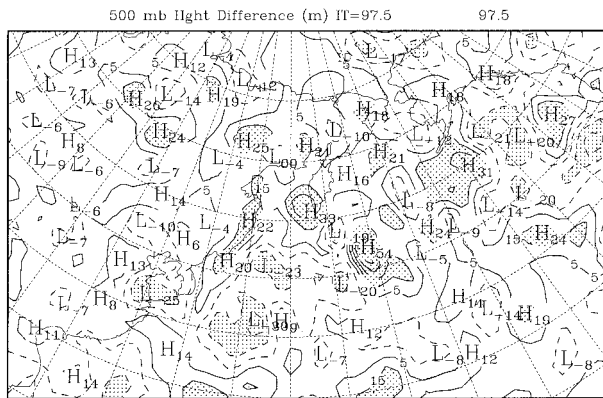


FIG. 5. Difference in initial 500-mb height (meters), ensemble members 14 minus 21 for initial time (IT) 97.5. Isopleths are every ± 5 m, ± 15 m, ± 25 m, . . . , with magnitudes above 15 m stippled.

and Du et al. (1997), and were designed to represent equally likely representations of the truth given typical analysis errors. An example of such perturbations, after initialization (Errico 1983), appears in Fig. 5 for the 500-mb height field at day 97.5, while the standard deviation for the perturbations about the ensemble mean appears in Fig. 6. The figures indicate that perturbations tend to be largest over the midlatitude storm tracks and near small-scale features such as short-wave troughs, and smallest over the continents and low latitudes, in accord with estimates of analysis uncertainty (Daley and Mayer 1986; Augustine et al. 1991; see Fig. 3a of Nutter et al. 1998).

4. Definition of verification and error

In presentation of results, it is necessary to measure error in the context of this long model run. In an operational environment, error is usually obtained by comparing the forecast against an observation or an analysis based on observations. Since this is not possible in the present case, as noted above, something from the model run itself must be used as verification. The two possibilities are the unperturbed run, which was used for the selection of the case, and an ensemble of analyses with initialized perturbations added to the unperturbed run for all verification times. Since by design the global average of the initial perturbations is zero (Mullen and Baumhefner 1989), these two measures will be approximately the same at the initial time. Moreover, since verification is needed *for times at which no initialized perturbations were generated* (i.e., days 98.0, 99.0, 100.0, and 101.0–102.5) and *for fields* (i.e., precipitation) that are not initially perturbed, the unperturbed run seems the most appropriate choice in this circumstance.

On the other hand, since the result of the unperturbed run would have been different had the initial conditions been perturbed and subsequently evolved by the model as described above, the unperturbed run has no claim

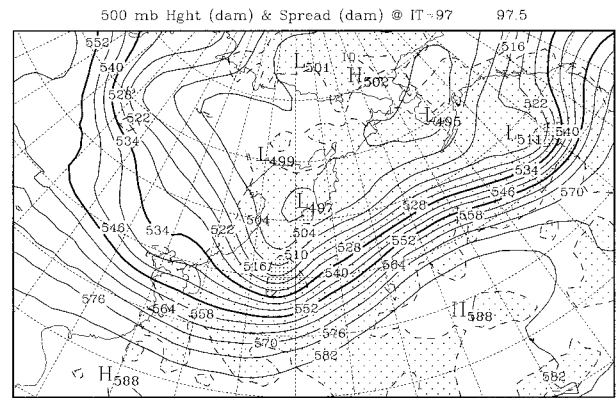


FIG. 6. Contours of initial ensemble-mean 500-mb height (solid), at intervals of 6 dam, for IT 97.5. Dashed lines are isopleths of rms value of 500-mb height perturbation after initialization, at intervals of 1 dam. Light stippling indicates values greater than 1 dam; heavy stippling indicates values greater than 2 dam.

to special consideration. Therefore, the error for all verification times is determined by cross validation (Wilks 1995, pp. 194–198), whereby each ensemble member in turn is taken as verification and compared against all remaining ensemble members, started from the same initial time. The results of these comparisons are then averaged and are considered as the error of the simulation.

The experimental design is patterned after the “perfect ensemble” system described by Buizza (1997), where one member is randomly selected to serve as verification for the remaining members. The perfect ensemble assumption maximizes skill, since model error is not considered and a perfect knowledge of analysis error statistics is assumed. When interpreting the results of this paper, the reader should kept in mind that our experiment yields an estimate of an upper bound on ensemble accuracy.

5. The ensemble simulations

a. Simulations for the Kamchatka cyclone

Histograms of central pressure for the Kamchatka cyclone in the 31 runs (the single unperturbed and 30 perturbed cases) appear in Fig. 7. A deep center was found in every run, ranging from 960 to 920 mb (to the nearest 5 mb) at a 5-day range, shrinking to a smallest range, from 955 to 930 mb at a 2-day range. The difference between extreme members oscillated with initial time, however, with a range (to the nearest 5 mb) of 40, 30, 40, and 25 mb at day 5 through day 2, respectively. The means and medians of central pressure exhibited similar behavior, gradually shifting toward weaker systems from day 5 to day 3 range (medians of 936, 944, and 952 mb, respectively), away from the unperturbed value of 934 mb, then abruptly jumping toward much deeper values at day 2 range (median of 939 mb). It is unclear whether this behavior has an underlying dy-

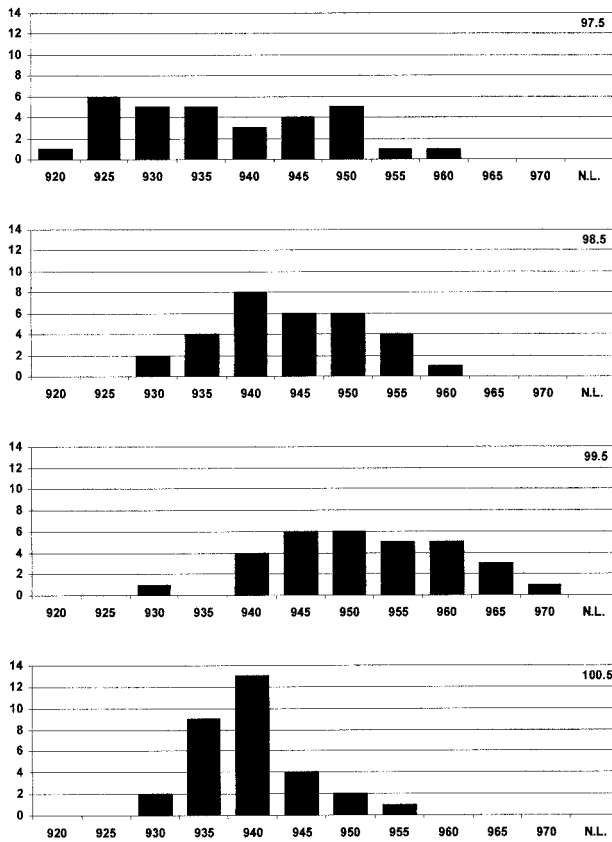


FIG. 7. Histograms of central pressure for the Kamchatka low at sea level to nearest 5 mb, for all 31 ensemble members at valid time (VT) 102.5. IT indicated in upper right side of each panel. The central pressure for the unperturbed cyclone is 934 mb.

namical cause, such as some earlier lead times being more sensitive to initial error than later ones, or represents a sampling fluctuation (ensemble size too small). The distributions at day 2 are consistent with the earlier results of Mullen and Baumhefner (1994) at coarser resolution. In the few weaker ensemble members at

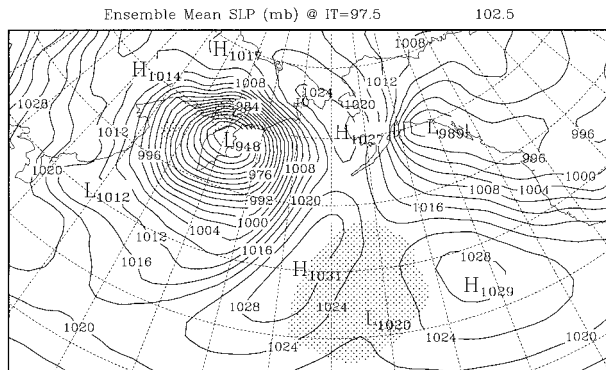


FIG. 8. Ensemble-mean sea level isobars at intervals of 4 mb, for IT 97.5, VT 102.5. Stippling denotes regions where the ensemble variance exceeds the model's climatological variance. Latitude and longitude lines as in Fig. 1.

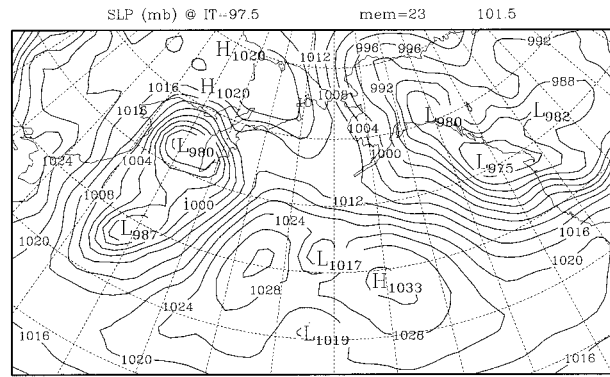


FIG. 9. Sea level isobars at intervals of 4 mb for member 23 starting at IT 97.5 valid at VT 101.5.

ranges of 3 and 4 days, the one-bergeron criterion of Sanders and Gyakum (1980) was not met during the 24-h period ending at day 102.5, but a significant low was nevertheless found. The ensemble-mean sea level pressure pattern at day 102.5, in the ensemble initiated five days earlier, appears as Fig. 8. The center is slightly northwest of the position in the unperturbed run, and the central pressure of 948 mb is less deep than the 936-mb median value. The reason for the discrepancy in position is that ensemble members with lower pressures lay northwest of the others. The difference in central pressure is due to variability of position of the center in the ensemble members.

There was also some variability within the ensemble in the mode of development of the system. In about half the members a low formed in an inverted trough near Taiwan at the beginning of the run and became a deepening system. Ensemble member 23 shows an example of this behavior. The low just east of Japan on day 101.5 (Fig. 9) initiated as a weak center at the northern tip of Taiwan 36 h earlier and ended with a central pressure of 920 mb west of Kamchatka 24 h later. In other instances, the low west of Kamchatka was the deeper throughout. An example is seen in Fig. 10, which produced the weakest low in the ensemble. The low over the Sea of Okhotsk remained the deepest on the map,

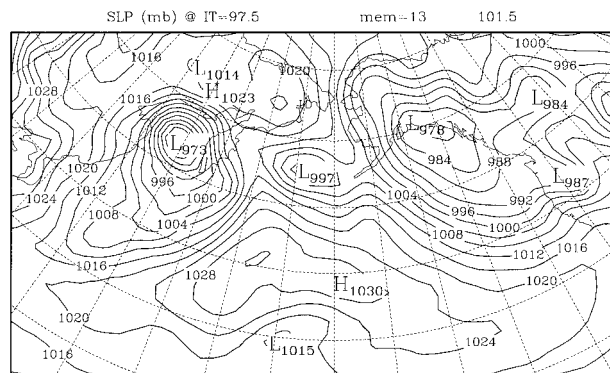


FIG. 10. Same as Fig. 9, but for member 13.

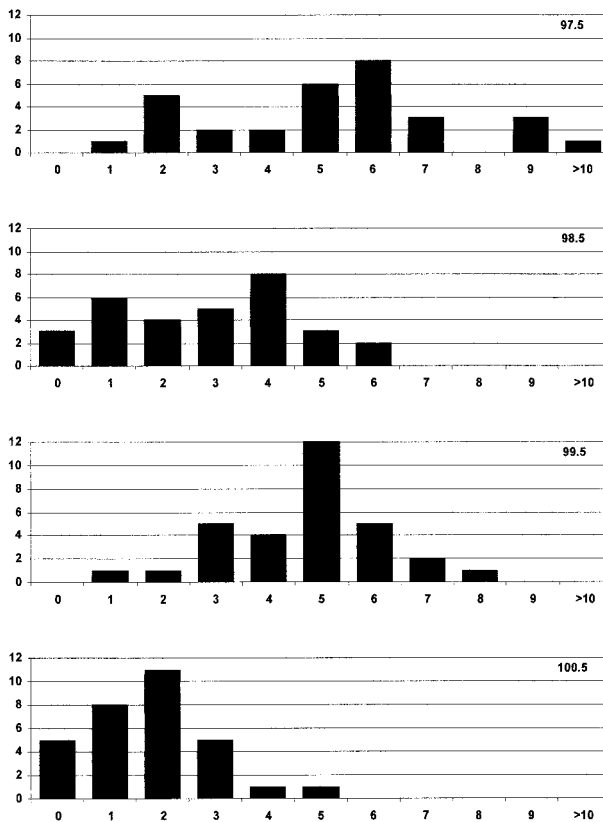


FIG. 11. Histograms of distances of center of Kamchatka low at sea level from position of ensemble mean low, in degrees of latitude (110 km), for all 31 ensemble at VT 102.5. IT is indicated in upper right side of each panel.

while the weak center over Taiwan never intensified significantly in this run. The model atmosphere, so to speak, knew where it wanted to go but was uncertain of the route taken to reach the goal. In those 16 members of the ensemble showing the deepest low south of 50°N latitude at some point in the run, the average final central pressure was about 933 mb, while in the 15 others the average was about 942 mb.

The variability of position of the final deep low within the ensembles is illustrated by the histograms in Fig. 11. The median distance of the centers in the individual ensemble members from the position of the ensemble-mean low shrank from about 5° latitude (550 km) at a range of 5 days to less than 220 km at 2-day range. Median distances at ranges of 5 and 3 days were virtually the same, presumably because of the influence of the low from Taiwan. The greatest difference in position for an ensemble member was about 1000 km in the run initiated at day 97.5.

b. Simulations for the central Pacific cyclone

The cyclone over the central Pacific displayed a different ensemble behavior. Although the unperturbed run showed a distinct and substantial center on day 102.5

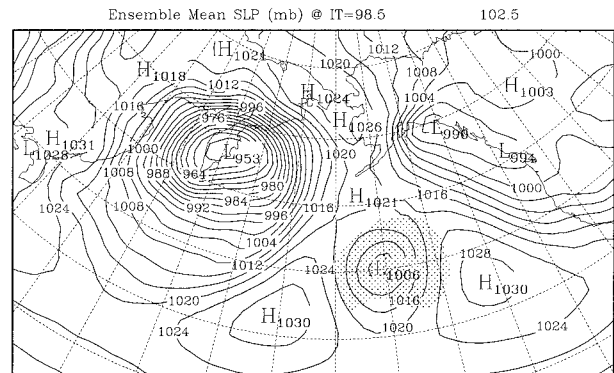


FIG. 12. Ensemble-mean sea level isobars at intervals of 4 mb, for IT 98.5 VT 102.5. Stippling denotes regions where the ensemble variance exceeds the climatological variance. Latitude and longitude lines as in Fig. 1.

(Fig. 1), the ensemble mean for this time initiated at day 97.5 showed a barely identifiable center in the region of col between two substantial anticyclones (Fig. 8). In the run initiated 24 h later (Fig. 12), there was a distinct center, albeit one still substantially less intense than that in the unperturbed run. This behavior appears to be an example in the ensemble mean fields of a “forecast fracture” (Sanders 1992), an abrupt difference in model solutions from consecutive runs valid at the same time. The comparison between the unperturbed run and the ensemble mean implies considerable variability among the ensemble members. Enhanced variability is also indicated in Figs. 8 and 12 by the stippling of regions where the standard deviation about the ensemble exceeds the climatic variance for the CCM2.

This variability is further confirmed by the histograms in Figs. 13 and 14. So far as central pressure is concerned, Fig. 13 shows a broad range of values. At 5-day range, two ensemble members had a central pressure near 1020 mb, as in the ensemble mean. The unperturbed run yielding 996 mb (Fig. 1) was one of the deeper members, although two others reached about 980 mb. The substantial number of “no-low” members at this 5-day range were determined subjectively on the basis of the absence of a low (no “L” symbol on a map) of significant depth within 1500 km of the position of the ensemble-mean low. The variability of positions and central pressures among the ensemble members shrank at the shorter ranges but remained substantially greater than the variability for the Kamchatka cyclone for all initial times. The difference in variability between the two cases is greatly enhanced when a comparison is made between the unperturbed or ensemble-mean values of the lows and the climatological mean values. The central pressure for the Kamchatka low is far below the climatological mean, while that for the central Pacific low is relatively close to it.

As examples of extremes of this variability in the runs initiated at day 97.5, we show maps of sea level pressure and 500-mb height for ensemble members 14 (Figs. 15

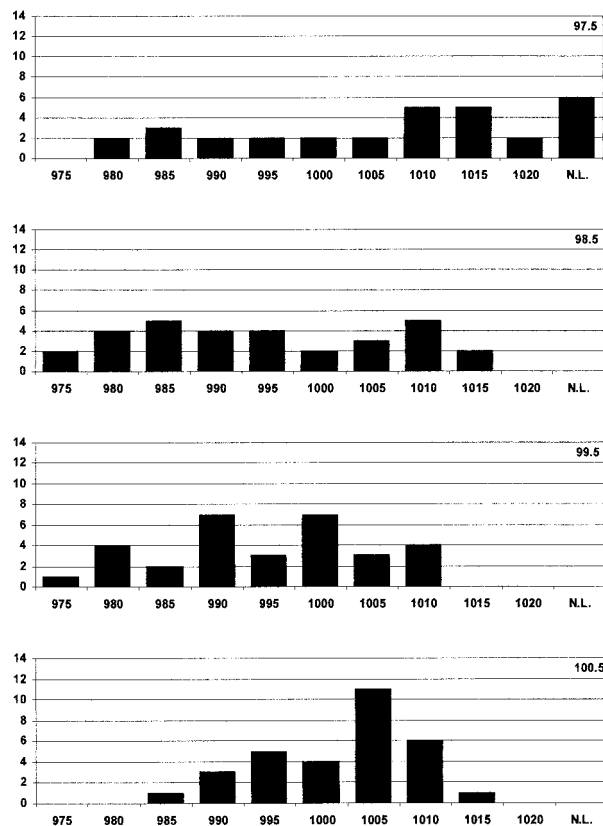


FIG. 13. Histograms of central pressure for the central Pacific low at sea level, to nearest 5 mb, for all 31 ensemble members at VT 102.5. IT is indicated in upper right side of each panel. NL means no low was present (see text). The central pressure for the unperturbed cyclone is 996 mb.

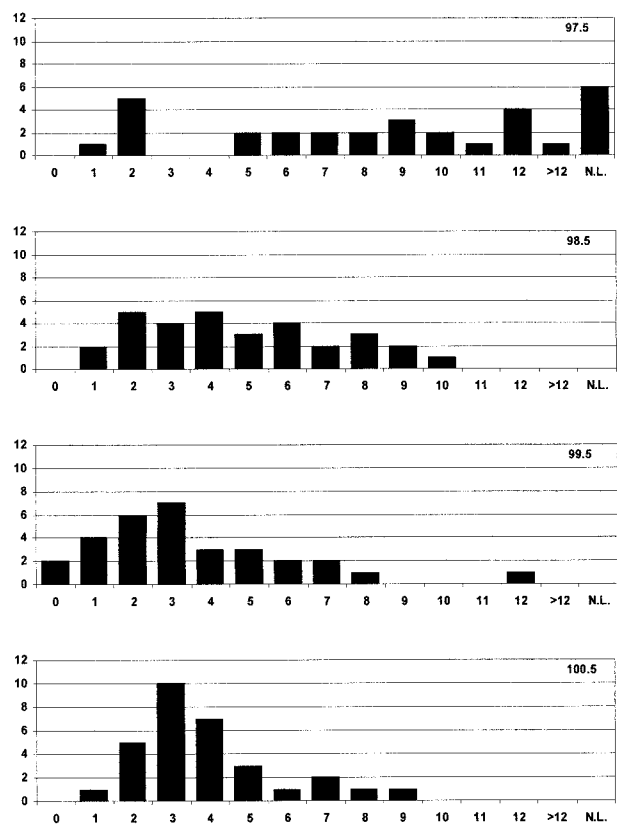


FIG. 14. Histograms of distance of the central Pacific low at sea level from position of ensemble mean low, in degrees of latitude (110 km), for all 31 ensemble members at VT 102.5. NL means no low was present. IT is shown in upper right side of each panel.

and 16) and 21 (Figs. 17 and 18). In the former pair there is a sea level cyclone over the central Pacific resembling that seen in the unperturbed run (Fig. 1) but considerably deeper. Aloft there is a pronounced trough with a weak low center, roughly coincident with the surface system. In contrast, member 21 displays at sea level a 1043-mb high slightly west of the low in Fig. 15, and no low at all within about 3000 km. At 500 mb, we see a less pronounced trough east of the surface high. Note that the position and central pressure of the low near Kamchatka varies relatively little (550 km and 10 mb, respectively) in these two ensemble members.

6. Difference in predictability

The difference in ensemble behavior between the two cyclones seems to imply something about smaller predictability for the Pacific storm.

If we can reliably assert that the probability of some event (of whatever character involving whatever weather element) is different from some “control” probability, then we can say we have some predictability of that event. The no-skill control in this case could be either persistence of the current condition or “climatology”

(the average condition suitably defined) or some simple combination of the two, such as persistence expectancy.

Let us now consider predictability of the sea level pressure field in our simulations. We say that the dispersion of the ensemble about its mean value is to be compared with the “climatological variance” at the same location, by which we mean the dispersion of daily

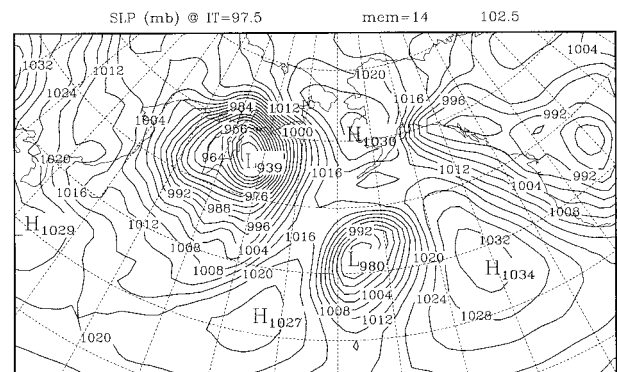


FIG. 15. Sea level isobars at intervals of 4 mb for ensemble member 14, IT 97.5 VT 102.5. Latitude and longitude lines as in Fig. 1.

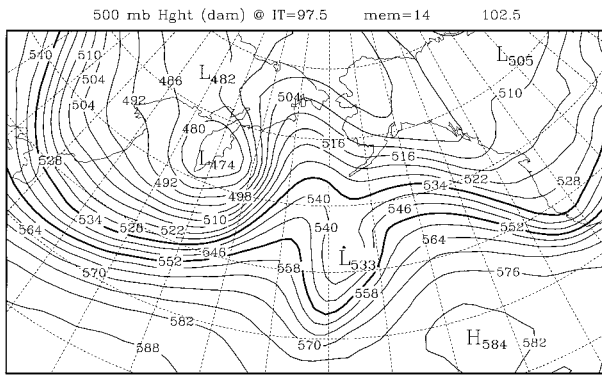


FIG. 16. Contours of 500-mb height, at intervals of 6 dam, for ensemble member 14, IT 97.5 VT 102.5.

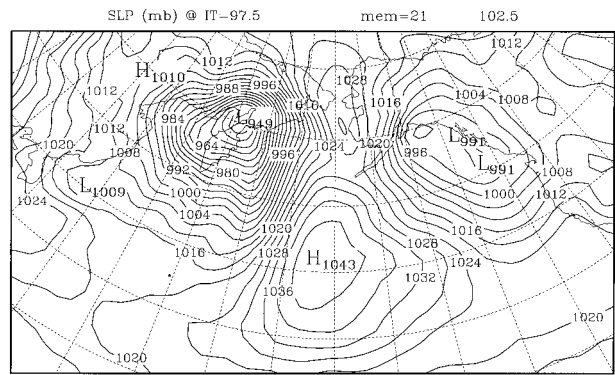


FIG. 17. Same as Fig. 16, but for ensemble member 21.

(or other) values about the mean during all or some part of the simulation run. If the variance of the ensemble is larger than the climatological variance at that location, we might say that there is no predictability in the sense that the average difference between two ensemble members exceeds the average difference between days selected at random from the climatological distribution. But this assertion neglects the fact that the verification may be far from the climatological mean value, as for example in the vicinity of the Kamchatka low, as opposed to the vicinity of the Pacific low, where verification is relatively close to the climatological mean. Hence, the probability distribution for the ensemble near Kamchatka (where the probability of a value below, say, 950 mb is much greater than its climatological value) may be quite different from the climatological distribution. Then the skill of the ensemble may be positive with respect to the climatological competitor, although the ensemble variance is larger than the climatological variance.

Some insight into the difference in behavior of these two systems in the ensemble can be obtained from Fig. 6. Over the western Pacific Ocean and eastern Asia on day 97.5, there were two major troughs at 500 mb. One of these was oriented nearly east–west over Siberia just north of latitude 60°N, while the other was oriented nearly meridionally just east of the Japanese islands. These were associated respectively with the development of the Kamchatka cyclone and the low in the Gulf of Alaska (not studied). The development of the low over the central Pacific was related to the weak trough in the northwesterly flow near 45°N, 100°E, just downwind of the Kamchatka trough. Figure 6 shows that the roof-mean-square (rms) value of the height perturbations over the Pacific was substantially greater than those over the Asian continent, reflecting the greater analysis uncertainty over the oceanic region of sparse data.

Since both troughs lay over the continental region of small uncertainty at day 97.5, however, a difference in the size of the initial perturbations is not a likely factor.

In fact, differences between the initial 500-mb analyses at day 97.5 for extreme members 14 and 21 (Fig. 5) were small. A similar sensitivity to small initial differences, as reflected in analyses from different operational centers, was obtained by Rabier et al. (1996, their Figs. 3 and 4) for a case of cyclogenesis over the North Atlantic. Rabier et al. (1996) show through linear adjoint analysis how small initial perturbations in dynamically sensitive regions can lead to widely divergent outcomes. In light of the analysis of Rabier et al., it is possible that our initial perturbations, which are *not* dynamically conditioned, project on such dynamically sensitive structures that were not quantified in this study.

On the other hand, the horizontal scales of the initial 500-mb troughs associated with the two systems, and with the subsequent upper-level troughs and surface lows, were quite different, substantially larger for the Kamchatka low. This initial 500-mb trough was much more pronounced than the trough associated with the central Pacific low. The large difference of outcome is also believed to be related, in part, to the different scales of the systems, reflecting their prominence as synoptic features.

As a measure of the difference in character of the two troughs, the initial maximum point geostrophic vorticity was obtained for each trough for each member of

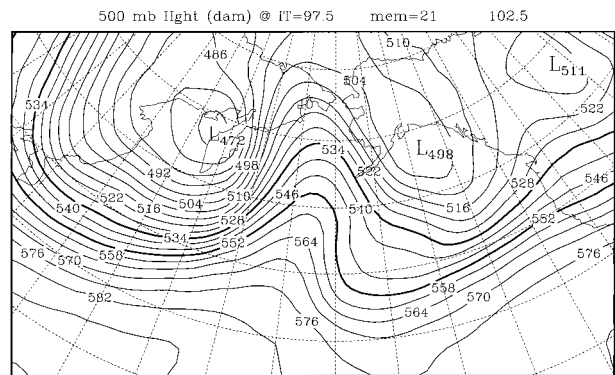


FIG. 18. Same as Fig. 17, but for ensemble member 21.

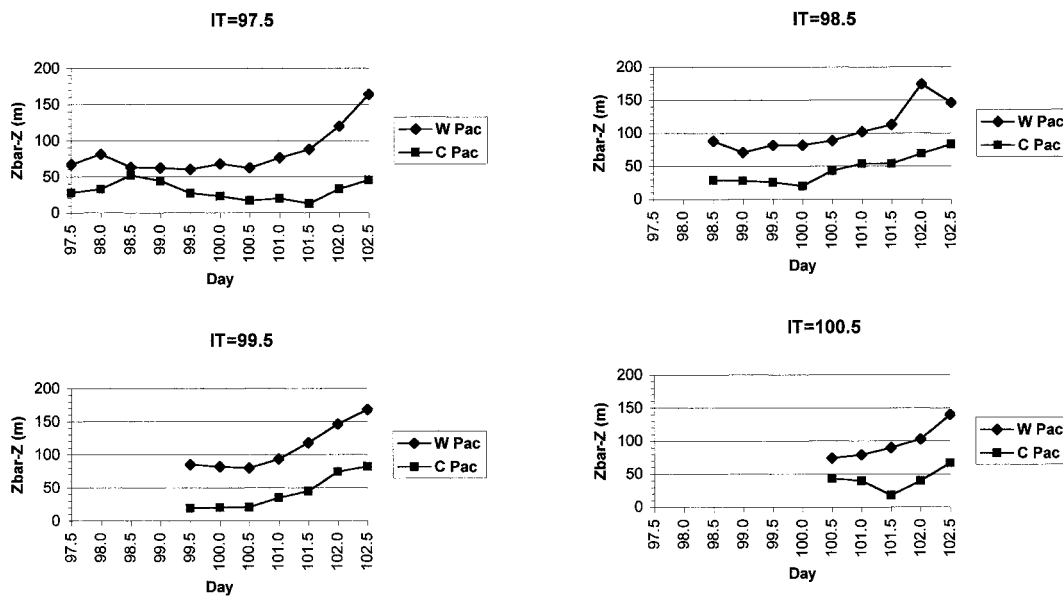


FIG. 19. Value of $Zbar - Z$, in m (see text), for maxima associated with the Kamchatka low (solid) and the central Pacific low (dashed) for the run starting at (upper left) day 97.5, (upper right) day 98.5, (lower left) day 99.5, and (lower right) day 100.5, valid at the day indicated along the abscissa.

the ensemble starting at day 97.5. The difference was modest. A better measure is the average vorticity over some area, as might be represented by the difference $Zbar$ minus Z , where $Zbar$ is the average value of Z at a certain averaging distance (660 km in our case) north, south, west, and east of a given point. This difference represents the average geostrophic vorticity over an area of width 660 km, centered on the given point. The point of maximum value was obtained for the ensemble mean for each trough at 12-h intervals, for each of the four ensembles. Results are plotted in Fig. 19, where the values for the more pronounced trough are larger than those for the weak trough by a factor of 2 or 3. For reference, the geostrophic area-mean relative vorticity is given, in units of 10^{-5} s^{-1} , by

$$6.196 \times 10^{-7} (\sin\varphi)^{-1} (Zbar - Z) \quad [\text{meters}],$$

where φ is the latitude. Thus the strong trough reaches a maximum value of 13.2 at day 102.5 in the run with IT 99.5, while the weaker trough reaches 9.1 at the same time.

A further point of interest in Fig. 19 is that development does not start immediately in all runs. In fact, a period of weakening precedes the period of rapid growth beginning around day 101. It is difficult to predict how altering the initial conditions for any of the ensembles would alter their subsequent behaviors. Note that both troughs, and especially the weaker one, suffer loss of strength while in a zone of broad-scale confluence at the entrance of the powerful Pacific winter jet. They grow in conjunction with cyclogenesis in the lower troposphere. This “self-development” is especially no-

table with the central Pacific system, where the scenario resembles that described by Hoskins et al. (1985).

The development of the two systems is illustrated by following the growth of the center of maximum dispersion of sea level pressure and 500-mb height associated with each. By dispersion or spread we mean the standard deviation from the appropriate ensemble average. Each system could be identified at the end of the run (on day 102.5) with a point of maximum ensemble spread. This feature was tracked back along the path of the system until it was no longer identifiable above the broad background value characterizing the initial conditions. These values are shown in Figs. 19 and 20 at 12-h intervals for the runs initialized at days 97.5, 98.5, 99.5, and 100.5. They are scaled for the two levels to be approximately equivalent. That is, an interval of 4 mb in sea level pressure yields about the same geostrophic wind as an interval of 30 m in 500-mb height.

Note that there is no rapid growth of dispersion, or total error for that matter, for either storm at either level until some time after the start of the run. The lack of data points for the early period of each run indicates the lack of a definite center that could be identified above the background level of dispersion, which is not much greater than the dispersion of initial conditions. For the Kamchatka low (Fig. 20) strong growth does not begin until about day 101, regardless of the initial time. Rapid growth for the central Pacific system (Fig. 21) begins about a day earlier. That the onset of vigorous growth begins at only a slightly later date in the later runs rather than at the same lag after the start indicates that the results reflect a real meteorological phenome-

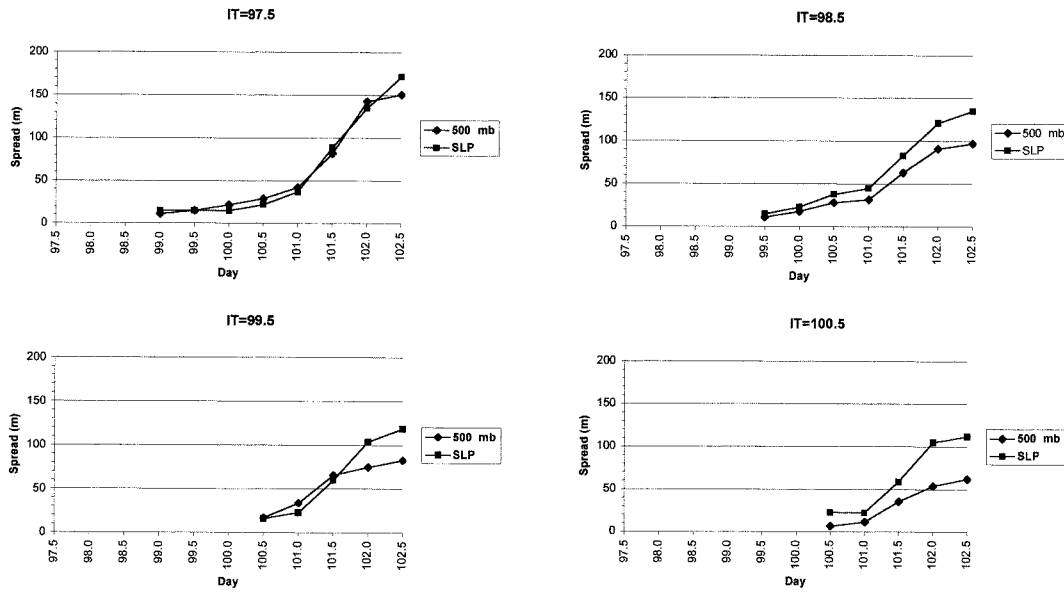


FIG. 20. Ensemble spread for the maximum associated with the Kamchatka low, for sea level pressure (in mb, solid) and for 500-mb height (in m, dashed) for the run starting at (upper left) day 97.5, (upper right) day 98.5, (lower left) day 99.5, and (lower right) day 100.5, and valid at the times shown along the abscissa.

non, likely related to the dynamic sensitivity of flow instabilities to initial perturbations. The dispersion by day 102.5, however, is not as large for the runs initiated later than for the earlier runs, and error growth continues to the end of each run, suggesting that further growth might have occurred had the later runs been carried farther. Once significant growth of dispersion begins, its doubling time is usually between half a day and one day, slightly less for the central Pacific storm. The reason for this difference in behavior is not known. The maximum dispersions reached for the central Pacific low are slightly larger than those for the Kamchatka system, despite its lesser strength in the ensemble mean, indicating less predictability for the former cyclone.

Further implications of reduced predictability are seen if these dispersions are compared with the deviation of the ensemble mean from the climatological mean. The values for the Pacific case are much larger, since the ensemble mean is relatively close to the climatological mean. Hence, the central Pacific development can be regarded as less predictable, as also indicated by the erratic occurrence of explosive deepening among the ensemble members.

Examination of the flow indicated by the Z bar fields shows that both vorticity maxima on day 97.5, particularly that for the central Pacific low, lay in the entrance region of a large-scale jet over the central Pacific (Fig. 22). The latter, already elongated along the flow, is stretched even farther because of conservation of vorticity in the confluent flow containing considerable deformation. Farrell (1989) has shown that a disturbance, elongated normal to the flow, would amplify in terms of disturbance energy and central deficit of stream-

function (or height) in such a confluent flow. His analysis, if applied to our situation of along-flow elongation in confluence, would no doubt indicate weakening of the disturbance, as we have seen. This confluence is present in all members of the ensemble but weakens as the disturbance travels eastward, vanishing around day 100, shortly before the onset of development in the unperturbed run as well as in those ensemble members yielding the most and least cyclogenesis over the central Pacific. We infer that the confluence inhibits development that might otherwise have occurred.

7. Types A and B cyclogenesis

This situation calls to mind the distinction drawn by Petterssen and Smebye (1971) between type A and type B cyclogenesis. They assert, *inter alia*, that in type A “development occurs under a more or less straight upper current (without appreciable vorticity advection)” and that “no cold upper trough is present initially, but one develops as the low-level cyclone intensifies; the distance of separation between the upper trough and the low-level cyclone remains sensibly unchanged until peak intensity is reached.” In contrast, with a type B event, “development commences when a pre-existing upper trough, with strong vorticity advection on its forward side, spreads over a low-level area of warm advection” and that “the distance of separation between the upper trough and the low-level system decreases rapidly while the cyclone intensifies.”

These scenarios, considered typical of the North Atlantic Ocean and North American continent, respectively, strongly resemble the developments in our en-

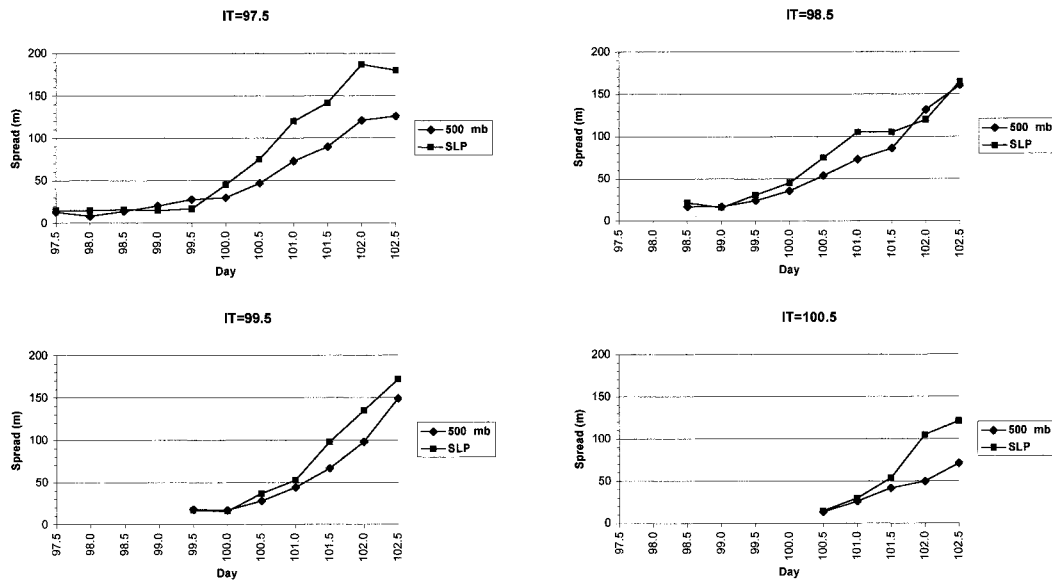


FIG. 21. Same as Fig. 20, but for the maximum associated with the central Pacific low.

semble simulations. The Kamchatka low is a prototypical type B development, while the central Pacific cyclogenesis, if not quite type A (because we know there was a weak initial upper-level predecessor) was at least a high B+. In a real situation in which the initial conditions is based on analysis of observations, the abundance of observations over the continents makes the identification of an upper trough quite easy, as they are nearly ubiquitous. Thus cyclogenesis is almost inevitably of type B. Over the oceans, on the other hand, the sparse coverage of data would likely fail to disclose the weak predecessor and would be characterized as a “more or less straight upper current.” The difficulty in finding a documented type A situation is thus no surprise: The weakness of the upper predecessor coupled

with the lack of oceanic data gives the impression that the B+ development is type A. In reality, type A may not exist. For a baroclinic development, if there was no upper-level predecessor and the system developed at all levels from infinitesimal beginnings, there would be no predictability at all. It is only the weak upper trough that allows the relatively small predictability in our central Pacific cyclone.

8. A scale partition

To explore further the issue of the dependence of dispersion growth on horizontal scale, we computed a localized growth, normalized by the CCM2’s climatological variance, for the unfiltered data, the large-scale waves (wavenumbers T10 and smaller), and the synoptic-scale waves (wavenumbers higher than T10). The T10 cutoff was chosen following Bottger (1988), who demonstrates the wintertime planetary wave features are adequately represented by wavenumbers T10 and lower. A quasi-Lagrangian calculation was done for all grid points, weighted by the cosine of latitude, within 10° latitude of the unperturbed positions of the surface low for the sea level pressure field and of the geostrophic vorticity maximum associated with surface development for 500-mb height field. For comparative purposes, we also calculated hemispheric values for the midlatitude region between 20° and 70°N. The results appear in Figs. 23 and 24 for the ensemble initialized at day 97.5. There are several noteworthy differences between the storm and hemispheric values, and between the central Pacific and Kamchatka lows.

At 500 mb (Fig. 23), the growth of the planetary waves does not deviate appreciably from the hemispheric value during the 5-day period, whereas the syn-

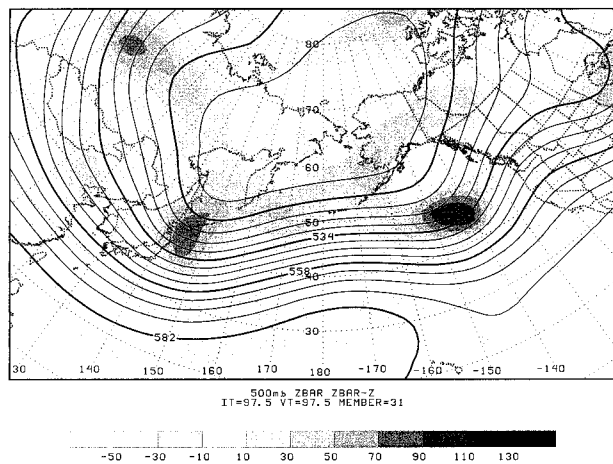


FIG. 22. Zbar and Zbar - Z, in m (see text), at intervals of 6 dam for the unperturbed run at IT 97.5. Values of Zbar - Z are shown by the scale at the left edge of the diagram.

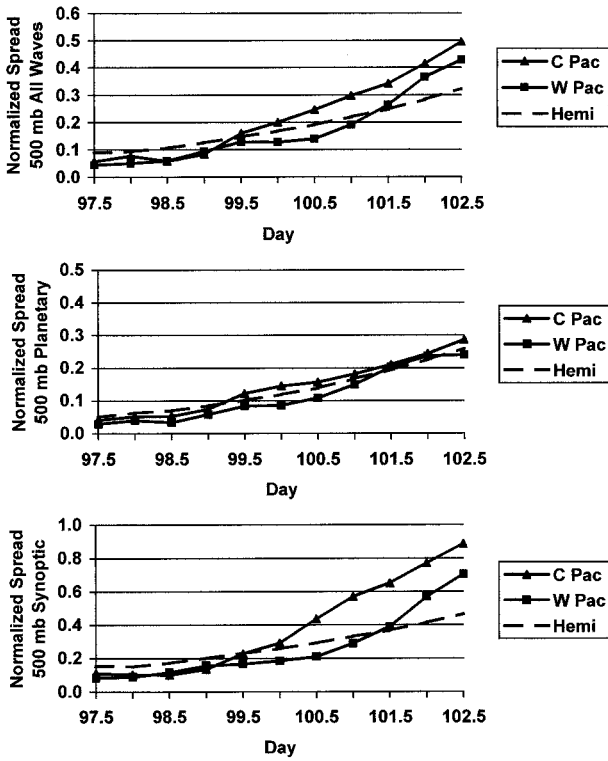


FIG. 23. Dispersion of 500-mb height in the run starting at day 97.5, normalized by the model climatic variance, for (top) unfiltered data, (middle) planetary waves, and (lower) synoptic waves. C Pac denotes dispersion for the central Pacific cyclone, W Pac the West Pacific cyclone, and Hemi the entire extratropical region from 20° to 70°N. See text for details.

optic scales do for both systems. The synoptic growth exceeds the hemispheric value a day earlier for central Pacific low and remains 0.2–0.3 units above the Kamchatka curve during the rapid deepening phase. Synoptic-scale doubling times for both troughs are around 24 h during the period of most rapid error growth, which coincides with or just precedes the period of most rapid surface intensification. Because the variance associated with planetary scales is much larger than for the synoptic scales, the total error growth for central Pacific trough runs only 0.1 units higher or less.

Differences at sea level (Fig. 24) are more pronounced. Like the 500-mb level, the synoptic variance exceeds the hemispheric background, but the deviation is far greater near the surface. Both curves saturate relative climatology, the Kamchatka low by day 102.5 and the central Pacific low nearly 48 h earlier. In fact, the central Pacific curve approaches the theoretical upper bound of square root of 2 by day 102.5 and thus appears to saturate. While the error growth in the planetary scales for Kamchatka low differs little from the hemispheric value, the central Pacific trough betters it by day 99.0 and reaches a value of 0.7 by day 102.5. Error doubling times during this period are typically 36 h. As a result, the total error for a few grid points near the

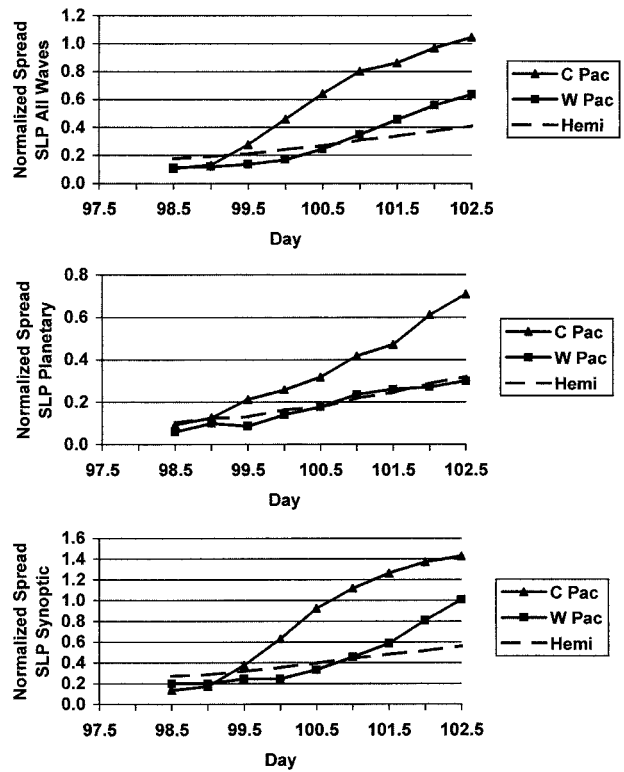


FIG. 24. Same as Fig. 23, but for sea level pressure.

center of stippled region of Fig. 8 becomes saturated by day 102.5. Difference between these results and those shown in Figs. 20 and 21 arise because not exactly the same quantities are being studied. In particular, Figs. 20 and 21 refer to point values while Figs. 23 and 24 refer to area averages centered on the cyclone.

The combination of rapid saturation of the synoptic scales and enhancement of the planetary wave error is responsible for the vast diversity of model solutions among the ensemble members at sea level. The rapid upscale growth of the planetary waves also suggests that a regime transition, such as into a blocked state or a persistent cutoff-low configuration, neither of which occurred in the unperturbed run, might be more likely within the immediate vicinity of this system, but that problematical forecast problem (e.g., Anderson 1993; Bottger 1988; Colucci and Baumhefner 1998; Tibaldi and Molteni 1990; Tibaldi et al. 1995; Tracton 1990) was not studied here.

We note that the rapid error growth and amplified dispersion in the synoptic scales first appear at sea level for both cyclones and that they remain bigger than the values at 500 mb throughout the surface development. Such a tendency is suggestive of an upward-directed growth of the normalized error and seems consistent with the vertical propagation of wave activity in numerical experiments of nonlinear baroclinic development (Hoskins 1983, his Fig. 7.5). An analysis of more

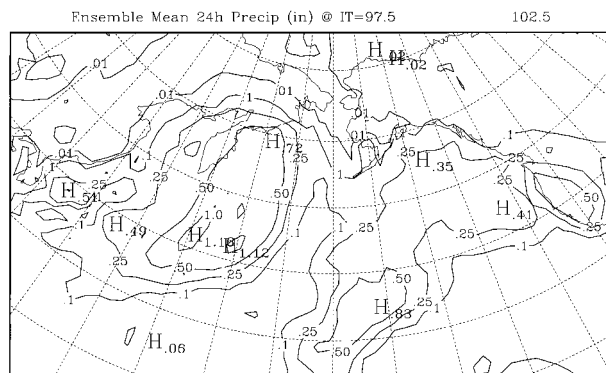


FIG. 25. Ensemble mean precipitation (in.) accumulated in preceding 24 h, IT 97.5 VT 102.5.

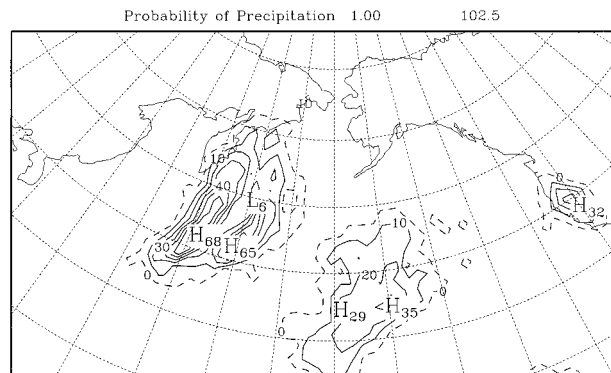


FIG. 26. Probability (%) of 24-h accumulated precipitation at least 1.00 in., derived from the relative frequency within the ensemble, for IT 97.5 VT 102.5. Dashed line represents 0% contour.

cases and vertical levels is obviously required before definitive conclusions can be reached.

9. Ensemble prediction of 24-h precipitation

From the point of view of the some users, sea level pressure and 500-mb height hold little interest. We therefore present some information on the precipitation produced by the ensemble. The ensemble-mean 24-h precipitation for the 24-h period ending at day 102.5, in the run initiated at day 97.5, appears in Fig. 25. A broad region of heavy rain, with maximum amounts slightly more than 1 in., extends from just northeast of the Kamchatka low to the southwestward, ahead of what would conventionally be regarded as the cold frontal trough (Fig. 12). This feature is consistent with synoptic experience. The large region over 0.50 in., would come as a surprise, given the weakness of the pressure field in Fig. 12, if we knew nothing of the ensemble variability. If the relative frequency of occurrence of at least 1.00 in. in the members of the ensemble is regarded as a probability, then the distribution shown in Fig. 26 ensues. Two meridional bands, with maximum probabilities greater than 60% and separated by approximately 500 km, lie ahead of the cold frontal trough south of the Kamchatka low and are related to a tendency for bimodality in frontal position among the individual ensemble members. The probability as high as 35% over the central Pacific would likely come as a surprise given the innocuous ensemble-mean, sea level pressure pattern there.

Precipitation amounts were placed in one of a set of mutually exclusive and exhaustive categories with zero and lower bounds at 0.01, 0.10, 0.25, 0.50, 1.00, and 2.00 in. These thresholds are important in operational forecasting of quantity of precipitation (QPF). The simulations were then verified by cross validation (Wilks 1995). Each of the 31 ensemble members was taken as "truth" and the rank probability skill score (RPSS) of Epstein (1969) and Murphy (1971) was applied to re-

maining members. The skill was measured with respect to the climatology of the simulation run, determined from the relative frequency of occurrence of each precipitation category at each grid point between days 46.0 (15 November) and 165.0 (14 March) of the simulation. The average skill for the 31 members appears as Fig. 27. Comparison with Fig. 25 shows that the highest skills (1.0 or nearly so) were found in regions where little or no precipitation occurred in the ensemble mean. In the region of heavy, ensemble-mean precipitation associated with the Kamchatka low, there were some areas of modest (0.5–0.0) skill. Over the central Pacific, there is no skill over the region of heavy ensemble-mean precipitation. Area-averaged RPSS values [Wilks 1995, Eq. (7.35)] for the North Pacific Basin (65°–25°N, 140°E–140°W), valid on day 102.5, are 0.31, 0.23, 0.33, and 0.40 for initial times of days 97.5 to 100.5, respectively. Thus, the precipitation simulations are globally skillful. The skill thus determined depends, of course, on the consistency of the precipitation among the members of the ensemble.

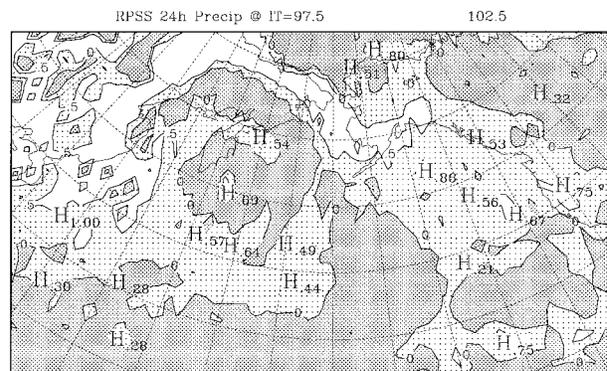


FIG. 27. RPSS for accumulated precipitation probability distribution with categories beginning at 0.01, 0.10, 0.25, 0.50, 1.00, and 2.00 in., IT 97.5 VT 102.5. Skill is with respect to the model's climatology (see text). Dark shaded area represents no skill, light shading 0.0 to 0.5, unshaded more than 0.5.

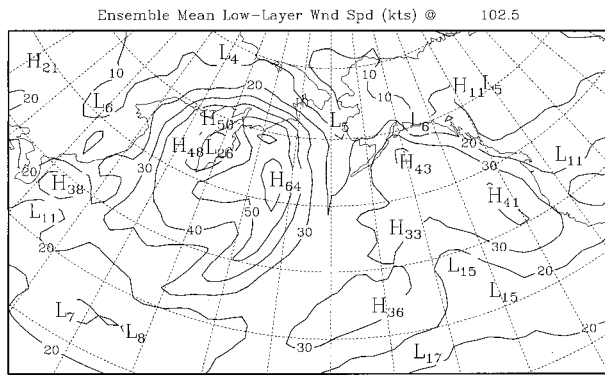


FIG. 28. Ensemble mean surface wind speed in knots for IT 97.5 VT 102.5.

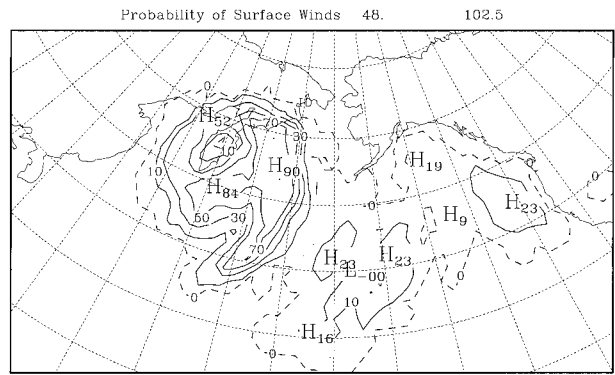


FIG. 29. Probability (%) of surface wind speed greater than 48 kt (storm force), derived from the relative frequency of occurrence in the ensemble, for IT 97.5 VT 102.5. The dashed line represents the 0% contour.

10. Ensemble prediction of low-level wind speed

We now examine wind speed at the lowest model level, about 8 mb (65 m) above the surface, for day 102.5 in the run initialized at day 97.5. The ensemble mean, representing the average of all the members, appears as Fig. 28. Comparison with the ensemble-mean pressure field (Fig. 8) shows less than perfect correspondence with the geostrophic wind. There is a region in Fig. 28 approaching hurricane force south and east of the Kamchatka center, but the area of extremely strong pressure gradient northwest through northeast of the center shows only modest winds in Fig. 28, reflecting the effects of stronger surface friction over the land and of cyclonic curvature in the isobars and low-level air trajectories. Contrariwise, the region of moderately strong wind in Fig. 28 over the central Pacific, where Fig. 8 shows only weak geostrophic flow, suggests large variability in the pressure gradient among the ensemble members.

The probability of winds of storm force (at least 48 kt or 24.7 m s^{-1}) was obtained from the relative frequency within the ensemble and appears as Fig. 29. The isobars in Fig. 8 make it easy to understand the area of large probability east and southeast of Kamchatka, but not the area of modest probability over the central Pacific. As with the precipitation simulations, probabilities provide a clear sign pointing to the large variability within the ensemble in this region. Note especially the local maximum of probability near 41°N , 169°W , where the gradient of the ensemble mean isobar field (Fig. 8) suggests a minimum in the wind speed.

As with the precipitation fields, the wind speeds were evaluated by applying the RPSS. The wind speed at each grid point was categorized into one of a set of exhaustive and mutually exclusive categories with lower bounds at 0, 18 kt (9.3 m s^{-1}), 34 kt (17.5 m s^{-1}), 48 kt and 64 kt (33.0 m s^{-1}). These thresholds (small craft advisory, gale, storm, and hurricane force) are important in operational marine forecasting. The ensemble was verified, as in the case of QPF, by cross validation. The climatological probabilities were derived as for the precipi-

tation categories. Results of this process appear in Fig. 30. Note that regions of substantial skill (0.5 and higher) appear in parts of the subtropics and in regions of light wind in the far north and northwest portions of the map area. South and east of Kamchatka some regions of moderate skill appear, due to consistency among members of the ensemble in these regions. Very little skill is found over the central Pacific, where the dispersion of the ensemble is large. The area-averaged RPSS values over the North Pacific basin at VT = 102.5 are 0.35, 0.43, 0.46, and 0.57 for initial dates of days 97.5 to 100.5, sequentially. These values show global skill and run 0.1–0.2 units higher than the precipitation values.

11. Concluding summary

We have examined the sensitivity of explosive cyclogenesis to initial condition uncertainty in a lengthy simulation run of the NCAR CCM2 model. We focused on day 102.5 of this run, when the deepest low appeared. An ensemble of 31 members was obtained by adding to the unperturbed simulation 30 runs starting from

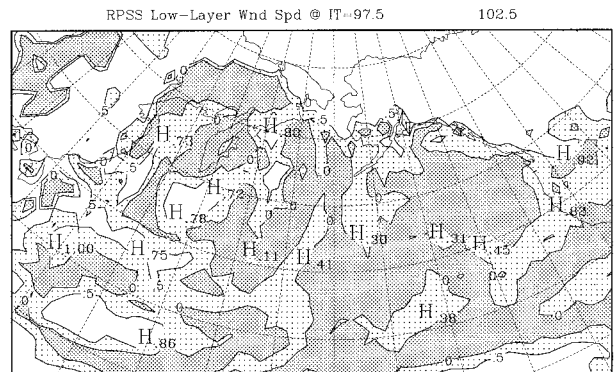


FIG. 30. RPSS for the ensemble forecast of categories of surface wind above 0, 18, 34, 48, and 64 kt, IT 97.5 VT 102.5, based on relative frequency of occurrence within the ensemble and verified against model's climatology (see text). Shading as in Fig. 27.

slightly perturbed initial conditions on days 97.5, 98.5, 99.5, and 100.5. The randomly generated perturbations contain amplitudes and scale-dependent, spatially correlated structures consistent with the prior estimates of analysis uncertainty (Daley and Mayer 1986; Augustine et al. 1991; Nutter et al. 1998).

An intense low near Kamchatka developed in each member of the ensemble, but the details of surface development varied from member to member. In contrast, a case of cyclogenesis over the central Pacific, marginally explosive, occurred in some members of the ensemble but not at all in others. Dispersion of the members about the ensemble mean and of the ensemble median increased irregularly with range. The difference in behavior of the two systems seems partially attributable to the strength of the respective predecessor trough at 500 mb or, put another way, to a localized enhancement of the error growth of the planetary and synoptic scales and to a difference in horizontal scale. Error growth was suppressed while the 500-mb vorticity feature was deformed in the entrance of the Pacific winter jet. The weakness of the vorticity center for the Pacific case gives the mistaken impression of being a type A development. The comparison shows that each cyclone had its own unique predictability characteristics and in general that the predictability of baroclinic developments can differ greatly.

Distributions of QPFs and surface wind speeds produced by the ensemble showed moderate to high skill out to day 5, but mainly away from the regions of most vigorous synoptic activity. Skill would undoubtedly be reduced if our assumption of a perfect ensemble was relaxed, as would be the case for an operational forecast verified against observations.

In a future study, it would be of interest to quantify relationships between ensemble dispersion and flow sensitivity for this case and other explosive developments. Valuable, quantitative insight into cyclone sensitivities has been obtained from recent applications of adjoint models, which can be used to define optimal initial perturbations and examine model sensitivities for a prescribed norm and finite time interval *within a linear framework* (e.g., Errico and Vukicevic 1992; Langland et al. 1996; Rabier et al. 1996; Errico and Raeder 1999). We note that present-day, adjoint sensitivity techniques may be less useful in testing sensitivities for a cyclogenesis such as the central Pacific low, however, because of the linearity assumption. The central Pacific low clearly undergoes strong nonlinear growth during its development: by day 4–5, the ensemble dispersion saturates for the synoptic scales and exceeds the climatic variance for unfiltered data, and the size of the evolved initial perturbations is comparable to those associated with the unperturbed cyclone itself. Moreover, some members exhibit greater than 2.00 in. of rain in 24 h, so latent heat release denotes a first-order process that must also be carefully considered in any adjoint sensitivity analysis (e.g., Langland et al. 1996; Errico and

Raeder 1999). We believe that this case points to the need of exploring the possibility of extending adjoint concepts into the nonlinear regime for models with realistic physics.

We close by recommending that the synthesis and display of output from operational ensemble forecast systems receive additional attention. Some of the pictorial displays that were used to summarize ensemble behavior in this paper could be tested to see if they might help forecasters to discern uncertainty in a synoptically relevant manner. For example, interactive histograms of cyclone tracks and central pressures from the ensemble could be implemented into computerized analysis and display systems through use of objective tracking algorithms (e.g., Sinclair 1994; Lefevre and Nielsen-Gammon 1995). In addition, the normalization of the ensemble spread by climatic variance, in conjunction with spatial–temporal decomposition of ensemble fields, offers a way to alert forecasters to times when scale-dependent details on the evolution of individual ensemble members should be viewed with caution.

Acknowledgments. The authors gratefully acknowledge the reviewers for their thorough and thought provoking reviews of the manuscript. Their comments lead to numerous improvements in the paper. The authors also thank Mr. Paul Nutter for his assistance with the computer simulations. FS thanks the Department of Atmospheric Science, The University of Arizona, for support during his annual visit. This work is supported by the National Science Foundation (NSF) through Grants ATM-9328752 and ATM-9712925 (FS), and ATM-9419411 and ATM-9714397 (SLM). The simulations were run on facilities of the Scientific Computing Division of the National Center for Atmospheric Research (NCAR); NCAR is supported by the NSF.

REFERENCES

- Anderson, J. L., 1993: The climatology of blocking in a numerical forecast model. *J. Climate*, **6**, 1041–1056.
- Augustine, S. J., S. L. Mullen, and D. P. Baumhefner, 1991: Examination of actual analysis differences for use in Monte Carlo forecasting. Preprints, *16th Annual Climate Diagnostics Workshop*, Los Angeles, California, NOAA/NWS/NMC/CAC, 375–378.
- Bottger, H., 1988: Forecasts of blocking and cyclone developments—Operational results during the winter of 1986/87. *Seminar on The Nature and Prediction of Extratropical Weather Systems*, ECMWF, 317–327. [Available from the European Centre for Medium-Range Weather Forecasts, Shinfield Park, Reading RG2 9AX, United Kingdom.]
- Buizza, R., 1997: Potential forecast skill of ensemble prediction and spread and skill distributions of the ECMWF ensemble prediction system. *Mon. Wea. Rev.*, **125**, 99–119.
- Colucci, S. J., and D. P. Baumhefner, 1996: Numerical prediction of the onset of blocking: A case study with forecast ensembles. *Mon. Wea. Rev.*, **126**, 773–784.
- Daley, R., and T. Mayer, 1986: Estimates for global analysis error from the global weather experiment observational network. *Mon. Wea. Rev.*, **114**, 1642–1653.
- Du, J., S. L. Mullen, and F. Sanders, 1997: Short-range ensemble

- forecasting of quantitative precipitation. *Mon. Wea. Rev.*, **125**, 2427–2459.
- Errico, R. M., 1983: A guide to transform software for non-linear normal-mode initialization of the NCAR Community Forecast Model. NCAR Tech. Note NCAR/TN-217+IA, National Center for Atmospheric Research, Boulder, CO, 86 pp.
- , and D. P. Baumhefner, 1987: Predictability experiments using a high-resolution limited-area model. *Mon. Wea. Rev.*, **115**, 488–504.
- , and T. Vukicevic, 1992: Sensitivity analysis using an adjoint of the PSU-NCAR mesoscale model. *Mon. Wea. Rev.*, **120**, 1644–1660.
- , and K. D. Raeder, 1999: An examination of the accuracy of the linearization of a mesoscale model with moist physics. *Quart. J. Roy. Meteor. Soc.*, **125**, 169–195.
- Epstein, E. S., 1969: Stochastic dynamic prediction. *Tellus*, **21**, 739–759.
- Farrell, B. F., 1989: Transient development in confluent and diffluent flow. *J. Atmos. Sci.*, **21**, 3279–3288.
- Hack, J. J., B. A. Boville, B. P. Briegleb, J. T. Kiehl, P. J. Rasch, and D. L. Williamson, 1993: A description of the NCAR Community Climate Model (CCM2). NCAR Tech. Note 382+STR, NCAR, Boulder, CO, 108 pp.
- Hoskins, B. J., 1983: Modelling of transient eddies and their feedback on the mean flow. *Large-Scale Dynamical Processes in the Atmosphere*, B. J. Hoskins and R. P. Pearce, Eds., Academic Press, 397 pp.
- , M. E. McIntyre, and A. W. Robertson, 1985: On the use and significance of isentropic potential vorticity maps. *Quart. J. Roy. Meteor. Soc.*, **111**, 877–946.
- Kallen, E., and X.-Y. Huang, 1988: The influence of isolated observations on short-range numerical weather forecasts. *Tellus*, **40A**, 324–336.
- Kuo, Y.-H., and S. Low-Nam, 1990: Prediction of nine explosive cyclones over the western Atlantic with a regional model. *Mon. Wea. Rev.*, **118**, 3–25.
- Langland, R. H., R. L. Elsberry, and R. M. Errico, 1996: Adjoint sensitivity of an idealized extratropical cyclone with moist physical processes. *Quart. J. Roy. Meteor. Soc.*, **122**, 1891–1920.
- Lefevre, R. J., and J. W. Nielsen-Gammon, 1995: An objective climatology of mobile troughs in the Northern Hemisphere. *Tellus*, **47A**, 638–655.
- Lorenz, E. N., 1982: Atmospheric predictability experiments with a large numerical model. *Tellus*, **34**, 505–513.
- Mullen, S. L., and D. P. Baumhefner, 1988: The sensitivity of numerical simulations of explosive oceanic cyclogenesis to changes in physical parameterizations. *Mon. Wea. Rev.*, **116**, 2289–2339.
- , and —, 1989: The impact of initial condition uncertainty on numerical simulations of large-scale explosive cyclogenesis. *Mon. Wea. Rev.*, **117**, 2800–2821.
- , and —, 1994: Monte Carlo simulations of explosive cyclogenesis. *Mon. Wea. Rev.*, **122**, 1548–1567.
- Murphy, A. H., 1971: A note on the Ranked Probability Score. *J. Appl. Meteor.*, **10**, 155–156.
- Nutter, P. A., S. L. Mullen, and D. P. Baumhefner, 1998: The impact of initial condition uncertainty on numerical simulations of blocking. *Mon. Wea. Rev.*, **126**, 2482–2502.
- Petterssen, S., and S. Smebye, 1971: On the development of extratropical cyclones. *Quart. J. Roy. Meteor. Soc.*, **97**, 457–482.
- Rabier, F., E. Klinker, P. Courtier, and A. Hollingsworth, 1996: Sensitivity of forecast errors to initial conditions. *Quart. J. Roy. Meteor. Soc.*, **122**, 121–150.
- Sanders, F., 1986: Explosive cyclogenesis in the west-central North Atlantic Ocean. Part I: Composite structure and mean behavior. *Mon. Wea. Rev.*, **114**, 1781–1794.
- , 1992: Skill of operational models in cyclone prediction out to five days during ERICA. *Wea. Forecasting*, **7**, 3–25.
- , and J. R. Gyakum, 1980: Synoptic-dynamic climatology of the “bomb.” *Mon. Wea. Rev.*, **108**, 1590–1606.
- , and S. L. Mullen, 1996: The climatology of explosive cyclogenesis in two general circulation models. *Mon. Wea. Rev.*, **124**, 1948–1954.
- Sinclair, M. R., 1994: An objective cyclone climatology for the Southern Hemisphere. *Mon. Wea. Rev.*, **122**, 2239–2256.
- Tibaldi, S., and F. Molteni, 1990: On the operational predictability of blocking. *Tellus*, **42A**, 343–365.
- , P. Ruti, E. Tosi, and M. Maruca, 1995: Operational predictability of winter blocking at ECMWF: An update. *Ann. Geophys.*, **13**, 305–317.
- Tracton, M. S., 1990: Predictability and its relationship to scale interaction processes in blocking. *Mon. Wea. Rev.*, **118**, 1666–1695.
- , and E. Kalnay, 1993: Operational ensemble prediction at the National Meteorological Center: Practical aspects. *Wea. Forecasting*, **8**, 379–398.
- Wilks, D. S., 1995: *Statistical Methods in the Atmospheric Sciences*. Academic Press, 467 pp.